Biomechan Model Mechanobiol (2007) 6: 43–53
DOI 10.1007/s10237-006-0044-z

ORIGINAL PAPER

W. Wilson · J. M. Huyghe · C. C. van Donkelaar

Depth-dependent compressive equilibrium properties of articular cartilage explained by its composition

Received: 14 July 2005 / Accepted: 23 November 2005 / Published online: 19 May 2006

Abstract For this study, we hypothesized that the depth-dependent compressive equilibrium properties of articular cartilage are the inherent consequence of its depth-dependent composition, and not the result of depth-dependent material properties. To test this hypothesis, our recently developed fibril-reinforced poroviscoelastic swelling model was expanded to include the influence of intra- and extra-fibrillar water content, and the influence of the solid fraction on the compressive properties of the tissue. With this model, the depth-dependent compressive equilibrium properties of articular cartilage were determined, and compared with experimental data from the literature. The typical depth-dependent behavior of articular cartilage was predicted by this model. The effective aggregate modulus was highly strain-dependent. It decreased with increasing strain for low strains, and increases with increasing strain for high strains. This effect was more pronounced with increasing distance from the articular surface. The main insight from this study is that the depth-dependent material behavior of articular cartilage can be obtained from its depth-dependent composition only. This eliminates the need for the assumption that the material properties of the different constituents themselves vary with depth. Such insights are important for understanding cartilage mechanical behavior, cartilage damage mechanisms and tissue engineering studies.

W. Wilson
Department of Biomedical Engineering,
Eindhoven University of Technology,
WH 4.108, P.O. Box 513, 5600 Eindhoven, MB, The Netherlands

J. M. Huyghe
Department of Biomedical Engineering,
Eindhoven University of Technology,
WH 4.127, P.O. Box 513, 5600 Eindhoven, MB, The Netherlands

C. C. van Donkelaar (✉)
Department of Biomedical Engineering, WH 4.118,
Eindhoven University of Technology, P.O. Box 513,
5600 Eindhoven, MB, The Netherlands
E-mail: c.c.v.donkelaar@tue.nl
Tel.: +31-40-2473135
Fax: +31-40-2447355

1 Introduction

Articular cartilage functions as a load-bearing, low friction, wear resistant material in diarthrodial joints. It consists of a fluid-filled extra-cellular matrix, in which chondrocytes are dispersed. The mechanical function is highly dependent on the composition of the extra-cellular matrix, which primary consists of collagen fibrils and negatively charged proteoglycans. Due to the fixed charges of the proteoglycans (PG's), the cation concentration inside the tissue is higher than in the surrounding synovial fluid. This excess of ion particles leads to an osmotic pressure difference, which causes swelling of the tissue (Urban et al. 1979). The fibrillar collagen network resists straining and swelling pressures (Mow et al. 1991). This combination makes cartilage a unique, highly hydrated and pressurized tissue, enforced with a strained collagen network.

The distribution of the matrix components in articular cartilage is highly depth-dependent. The fluid fraction in articular cartilage is around 80% and decreases with increasing distance from the articular surface (Lipshitz et al. 1975; Shapiro et al. 2001; Rieppo et al. 2004). Collagen constitutes approximately 70% of the tissue dry weight (Buckwalter et al. 1991; Mow and Guo 2002; Rieppo et al. 2004), and is highest in the superficial and deep zones of articular cartilage, and lowest in the middle zone (Mow and Guo 2002; Rieppo et al. 2004; Rieppo et al. 2005). PG-molecules constitute approximately 20–30% of the total dry tissue weight (Buckwalter et al. 1991). The PG content is lowest in the superficial zone, and highest in the middle zone (Hunziker et al. 1992; Wong et al. 1996). Although the PG content is lower in the deep zone than in the middle zone, the fixed charge density (FCD) is highest in the deep zone (Maroudas 1968; Maroudas and Bannon 1981; Chen et al. 2001. As the PG content is expressed as mass percentage per dry weight and the FCD as mEq/ml, the low fluid fraction in the deep zone can explain the high FCD in this zone (Chen et al. 2001).

Apart from its composition, also the structure of articular cartilage is depth-dependent. In the superficial zone colla-

gen fibers are densely packed, and are arranged parallel to the articular surface (Benninghoff 1925; Hasler et al. 1999; Clark 1997; Clarke 1971). In the middle zone collagen fibers are more randomly arranged (Benninghoff 1925; Clark 1997; Clarke 1971; Hasler et al. 1999). In the deep zone the collagen fibers have their largest diameters and are arranged perpendicular to the subchondral bone (Benninghoff 1925; Hunziker et al. 1997; Hasler et al. 1999).

This depth-dependent composition and structure of the ECM results in depth-dependent mechanical properties. Schinagl et al. (1997) and Chen et al. (2001) have shown that the compressive equilibrium stiffness of articular cartilage increases with distance from the articular surface. Surprisingly they also found that while the stiffness of the top layers increased with increasing strain, the stiffness of the deep layers seemed to decrease with increasing strain. This strain softening has also been observed during unconfined compression (Chahine et al. 2004), and is associated with the osmotic swelling pressures which prestresses the tissue. For external compressive loads lower smaller than the swelling pressures the tissue is under tension and for external loads larger than the swelling pressures the tissue is under compression. As articular cartilage has a high compression-tension nonlinearity this can explain the strain-softening of the tissue (Chahine et al. 2004).

Several authors have attempted to correlate the compressive stiffness of articular cartilage to its composition. Although the aggregate modulus showed a good correlation with the fluid content (Armstrong and Mow 1982), GAG-content (Sah et al. 1997) and fixed charge density (Chen et al. 2001), the depth- and strain-dependent behavior of the aggregate modulus has not been explained solely based on tissue composition, yet. We hypothesize that this is due to an inaccurate approach in the description of the distribution of water in the tissue. So far, cartilage has been described as a porous material, filled with free water. The osmotic pressure is normally computed based on the number of fixed charged per milliliter of this free water (FCD). It has been shown, however, that the osmotic pressure inside cartilaginous tissues is much higher than would be expected based on its FCD (Meyer et al. 1983; Urban and McMullin 1988; Maroudas and Bannon 1981). This is because part of the water in the tissue is absorbed by the collagen fibers. The proteoglycan molecules, because of their large size, are excluded from this intra-fibrillar space. This means that their effective concentrations are much higher in the extra-fibrillar space than if they were distributed uniformly throughout the entire matrix (Urban and McMullin 1988; Maroudas and Bannon 1981; Katz et al. 1986; Maroudas et al. 1991). Hence, the effective fixed charge density is higher than if computed from total tissue water content. As the collagen content, and thereby the intra-fibrillar water content, is depth-dependent, the influence of intra- and extra-fibrillar water is also depth-dependent, resulting in an extra depth-dependency in the swelling pressures.

As the solid content increases from the superficial to the deep zone, the contribution of the solid matrix to the total tissue stiffness should increase from the superficial to the deep zone. Hence, besides differences in the swelling pressures over the height of the tissue, the compressive modulus is also depth-dependent. Till now this dependence of the matrix stiffness on its density has never been included in models of articular cartilage.

Although the solid itself is virtually incompressible, due to its porous structure, the entire solid matrix is compressible. If the fluid is fully expelled, the solid fraction is 1, and the entire matrix has become incompressible. Hence, the compressibility of the tissue should be dependent on the solid fraction. This introduces an additional depth-dependency, which is not included in regular multi-phasic models.

We hypothesized that (1) the depth-dependent compressive equilibrium properties of articular cartilage are the inherent consequence of the composition of the tissue, which changes with depth, and that (2) the inclusion of intra- and extra-fibrillar water and solid fraction dependency as discussed above are essential for the understanding of the depth-dependent behavior of articular cartilage. To test the hypotheses our recently developed fibril-reinforced poroviscoelastic swelling model (Wilson et al. 2005b) was expanded to include the influence of intra- and extra-fibrillar water content, and the influence of the solid fraction on the compressive properties of the tissue. With this model the depth-dependent compressive equilibrium properties of articular cartilage were determined, and compared with the experimental data of Schinagl et al. (1997).

2 Methods

2.1 Model

In the fibril-reinforced poroviscoelastic swelling theory (Wilson et al. 2005b) articular cartilage is assumed as biphasic, consisting of a solid and a fluid phase. The solid phase consists of a swelling non-fibrillar part, which contains mainly PG's, and a fibrillar part representing the collagen network.

2.1.1 Incorporation of solid fraction dependency

In the standard biphasic theory the total stress is given by

$$\boldsymbol{\sigma}_{\mathrm{tot}} = -p\mathbf{I} + \boldsymbol{\sigma}_{\mathrm{s}} = -pn_{\mathrm{s}}\mathbf{I} - pn_{\mathrm{f}}\mathbf{I} + \boldsymbol{\sigma}_{\mathrm{s}}, \tag{1}$$

where p is the hydrostatic pressure, $\boldsymbol{\sigma}_{\mathrm{s}}$ the effective solid stress, $\mathbf{I}$ the unit tensor, and n_{f} and n_{s} the fluid and solid volume fractions, respectively. Typically, the effective stress depends on strain only. Hence, the relative fluid and solid volume fractions do not influence the total stress in the tissue in Eq. 1. Hence, in the biphasic model (Mow et al. 1980) only the amount of deformation and not the amount of solid has an influence on the stress contribution of the solid matrix to the total tissue stress. If the solid fraction is accounted for, the total stress becomes

$$\begin{aligned}\boldsymbol{\sigma}_{\mathrm{tot}} &= -p\mathbf{I} + n_{\mathrm{s}}\boldsymbol{\sigma}_{\mathrm{rs}} = -p\mathbf{I} + \frac{n_{\mathrm{s},0}}{J}\boldsymbol{\sigma}_{\mathrm{rs}} \\ &= -p\mathbf{I} + n_{\mathrm{s},0}\boldsymbol{\sigma}_{\mathrm{rs},J}(J),\end{aligned} \tag{2}$$

where $n_{s,0}$ and n_s are the initial and current solid volume fraction, and J the volumetric deformation. Note that the dependency of the solid fraction on the volumetric deformation is included in the function for the real solid stress ($\boldsymbol{\sigma}_{rs,J}$).

When osmotic swelling is included the total tissue stress becomes

$$\boldsymbol{\sigma}_{tot} = -\mu^f \mathbf{I} + n_{s,0}\boldsymbol{\sigma}_{rs,J} - \Delta\pi \mathbf{I}, \tag{3}$$

where μ^f is the water chemical potential and $\Delta\pi$ the osmotic pressure gradient. In our previous papers (Wilson et al. 2004, 2005b) we used the following description for the solid stress

$$\boldsymbol{\sigma}_{rs,J} = \boldsymbol{\sigma}_{nf} + \sum_{i=1}^{tot\,f} \boldsymbol{\sigma}_f^i, \tag{4}$$

where $\boldsymbol{\sigma}_{nf}$ is the stress in the nonfibrillar matrix, and $\boldsymbol{\sigma}_f^i$ the fibril stress in the ith fibril with respect to the global coordinate system. In these models it was assumed that the fibril network is laid over the non-fibrillar matrix. Hence, the distinct volumes of the different components has not been accounted for. The easiest way to account for the different volumes is by using the mixture theory (Truesdell and Toupin 1960). This theory is based on the following assumptions (1) in each infinitesimal volume of the composite material a finite number of components are present; (2) each component contributes to the total material behavior in the same proportion as its volumetric participation; (3) all components have the same strains. When the rule of mixtures is used, the total solid stress becomes

$$\boldsymbol{\sigma}_{rs,J} = \left(1 - \sum_{i=1}^{tot\,f} \rho_c^i\right)\boldsymbol{\sigma}_{nf} + \sum_{i=1}^{tot\,f} \rho_c^i \boldsymbol{\sigma}_f^i, \tag{5}$$

with ρ_c^i the volume fraction of the collagen fibrils in the ith direction with respect to the total volume of the solid matrix. Note, that as the total solid is assumed to be incompressible, the relative fractions of the fibrillar and non-fibrillar matrix remain constant. With Eq. (5) the total tissue stress from Eq. (3) becomes

$$\boldsymbol{\sigma}_{tot} = -\mu^f \mathbf{I} + n_{s,0}\left(\left(1 - \sum_{i=1}^{tot\,f} \rho_c^i\right)\boldsymbol{\sigma}_{nf} + \sum_{i=1}^{tot\,f} \rho_c^i \boldsymbol{\sigma}_f^i\right) - \Delta\pi \mathbf{I}. \tag{6}$$

2.1.2 Fibrillar part

In our previous models (Wilson et al. 2004, 2005b) the stress contribution of fibrils contained in a unit area was given by

$$\boldsymbol{\sigma}_f = \sigma_f \vec{e}_f \vec{e}_f. \tag{7}$$

where $\boldsymbol{\sigma}_f$ is the Cauchy stress tensor, σ_f is the Cauchy stress in the fibril and the current fibril direction. The unit area on which σ_f acts does not contain a fixed number of fibrils at different times. Thereby, due to deformation the surface a fibril works on changes. So far, the influence of this surface change has not been included. To include this, the fibril stress is expressed with reference to its original state. The 2nd Piola–Kirchhoff stress tensor is then given by

$$\mathbf{S}_f = S_f \vec{e}_{f,0} \vec{e}_{f,0}, \tag{8}$$

where $\vec{e}_{f,0}$ is the initial fibril direction. The 2nd Piola–Kirchhoff stress in the initial fibril direction S_f is given by

$$S_f = \frac{P_f}{\lambda} = \frac{P_f}{\left\|\mathbf{F} \cdot \vec{e}_{f,0}\right\|}, \tag{9}$$

with λ the elongation of the fibril, $\mathbf{F}$ the deformation gradient tensor, and P_f the first Piola–Kirchhoff stress. The total Cauchy stress (expressed as a function of the deformed state) is then given by

$$\boldsymbol{\sigma}_f = \frac{1}{J}\mathbf{F} \cdot \mathbf{S}_f \cdot \mathbf{F}^T = \frac{1}{J}\frac{P_f}{\lambda}\mathbf{F} \cdot \vec{e}_{f,0}\vec{e}_{f,0} \cdot \mathbf{F}^T = \frac{\lambda}{J} P_f \vec{e}_f \vec{e}_f, \tag{10}$$

where J is the determinant of the deformation tensor $\mathbf{F}$. If the law for fibril stress is now expressed as the first Piola–Kirchhoff stress P_f (instead of the Cauchy stress σ_f) the only difference between Eq. (10) and Eq. (7) is the factor λ/J which represents the change in surface the fibril works on. Note that the factor $1/J$ from Eq. (2) is included in Eq. (10).

In our previous models the collagen fibrils were assumed to consist of an elastic part (representing the equilibrium properties) and a viscoelastic part (representing the transient properties) (Wilson et al. 2004, 2005b). As Schinagl et al. (1997) only measured the depth-dependent equilibrium properties, in this study we are only interested in the equilibrium properties of the tissue. Therefore, the viscoelastic part of the collagen fibrils is not included. The equilibrium stiffness of the collagen fibrils was previously assumed to be strain-independent (Wilson et al. 2004, 2005b). However, Charlebois et al. (2004) have shown that the equilibrium stiffness of the collagen fibrils is strain-dependent. Therefore, the collagen fibrils are now represented by:

$$\begin{aligned} P_f &= (E_1 + E_2\varepsilon_f)\varepsilon_f \quad \text{for } \varepsilon_f > 0, \\ P_f &= 0 \qquad\qquad\qquad\quad \text{for } \varepsilon_f \le 0, \end{aligned} \tag{11}$$

with ε_f the logarithmic fibril strain ($\varepsilon_f = \log(\lambda)$), and E_1 and E_2 are positive material constants. For the determination of the fibrils strains and directions, the reader is referred to (Wilson et al. 2004, 2005b).

2.1.3 Non-fibrillar part

For the behavior of the non-fibrillar solid matrix we previously used the following compressible neo-Hookean model (Wilson et al. 2005b),

$$\boldsymbol{\sigma}_{nf} = K_m \frac{\ln(J)}{J}\mathbf{I} + \frac{G_m}{J}(\mathbf{F} \cdot \mathbf{F}^T - J^{2/3}\mathbf{I}), \tag{12}$$

The bulk (K_m) and shear moduli (G_m) are defined as

$$K_m = \frac{E_m}{3(1 - 2\nu_m)}, \tag{13}$$

$$G_m = \frac{E_m}{2(1 + \nu_m)}, \tag{14}$$

where E_m is the Young's Modulus and ν_m the Poisson's ratio. Note that the influence for the volume change due to deformation as discussed earlier has been accounted for in Eq. (12) by the factor $1/J$.

Although the solid itself is virtually incompressible, due to its porous structure the entire solid matrix is compressible. If the fluid is fully expelled, the solid fraction is, and the entire matrix has become incompressible. As the solid fraction goes to zero the volume fraction of the pores goes to 1 and the entire solid matrix will become fully compressible. To include this in the model the following expression for the Poisson's ratio is proposed.

$$\nu_m = 0.5 n_s = 0.5 \frac{n_{s,0}}{J}, \tag{15}$$

Note that ν_m goes to 0.5 for a solid fraction of 1, and becomes zeros when the solid fraction goes to zero. By substituting Eq. (15) into Eq. (13) and (14), and by eliminating E_m we get the following expression for K_m

$$K_m = \frac{2}{3} G_m \frac{(1 + 0.5 n_{s,0}/J)}{(1 - n_{s,0}/J)}. \tag{16}$$

Because the second law of thermodynamics needs to be fulfilled, the constitutive relation for K_m cannot be directly substituted in Eq. (12). We therefore first implement it into the energy function of Eq. (12) and derive the new Cauchy stress from this energy function. The new energy function then becomes

$$\begin{aligned} W_{nf} &= \frac{1}{8} K_m \ln^2(\det(\mathbf{C})) + \frac{1}{2} G_m (\mathrm{tr}(\mathbf{C}) - 3\det(\mathbf{C})^{1/3}) \\ &= \frac{1}{12} G_m \frac{(1 + 0.5 n_{s,0}/J)}{(1 - n_{s,0}/J)} \ln^2(\det(\mathbf{C})) \\ &\quad + \frac{1}{2} G_m (\mathrm{tr}(\mathbf{C}) - 3\det(\mathbf{C})^{1/3}). \end{aligned} \tag{17}$$

where $\mathbf{C}$ is the Cauchy-Green deformation tensor. The Cauchy stress of the non-fibrillar matrix is then given by

$$\begin{aligned} \boldsymbol{\sigma}_{nf} &= \frac{2}{J} \mathbf{F} \frac{\partial W_{nf}}{\partial \mathbf{C}} \mathbf{F}^T \\ &= -\frac{1}{6} \frac{\ln(J)}{J} G_m \mathbf{I} \left[-1 + \frac{3(J + n_{s,0})}{(-J + n_{s,0})} + \frac{3 \ln(J) J n_{s,0}}{(-J + n_{s,0})^2} \right] \\ &\quad + \frac{G_m}{J} (\mathbf{F} \cdot \mathbf{F}^T - J^{2/3} \mathbf{I}). \end{aligned} \tag{18}$$

A similar approach has been used by Ehlers and Eipper (1999). To illustrate the importance of a solid fraction dependent compressibility, the responses of Eq. (12) and Eq. (18) during confined compression and extension are plotted in Fig. 1.

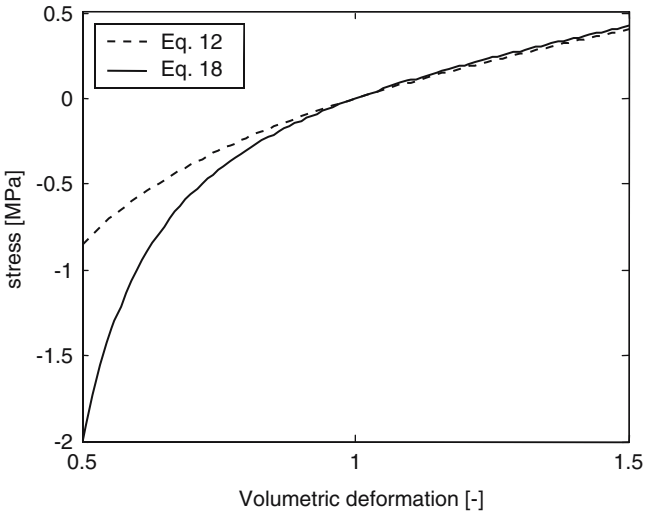

Fig. 1 Stress–strain behavior of the neo-Hookean model during confined compression and extension, with and without of solid fraction dependent compressibility ($n_{s,0} = 0.25$, $E = 1$ MPa and $\nu = 0.01$)

2.1.4 Osmotic swelling

For the swelling behavior the biphasic swelling theory (Wilson et al. 2005a,b) was used. This theory is based on the hypothesis that electrolyte flux can be neglected in mechanical studies of charged materials (Lanir 1987). This means the ion concentrations is assumed in equilibrium. The osmotic pressure gradient is then given by

$$\Delta\pi = \phi_{int} RT \left(\sqrt{c_F^2 + 4 \frac{(\gamma_{ext}^{\pm})^2}{(\gamma_{int}^{\pm})^2} c_{ext}^2} \right) - 2\phi_{ext} RT c_{ext}, \tag{19}$$

with c_{ext} the external salt concentration and c_F the FCD. The osmotic (ϕ_α) and activity coefficients (γ_α) were implemented as proposed by Huyghe et al. (2003). Note that the current FCD is a function of the volumetric deformation (J) of the tissue as

$$c_F = c_{F,0} \frac{n_{f,0}}{n_{f,0} - 1 + J}. \tag{20}$$

2.1.5 Inclusion of intra- and extra-fibrillar water

When the distinction between extra- and intra-fibrillar water is taken into account, the effective FCD should be expressed as mEq fixed charges per ml extra-fibrillar water. Hence, the effective FCD becomes

$$c_{F,exf} = \frac{n_f c_F}{n_{exf}}, \tag{21}$$

where the volume fraction of extra-fibrillar water n_{exf} is given by

$$n_{exf} = \frac{\rho_s n_{exf,m}}{1 - n_{exf,m} + \rho_s n_{exf,m}}, \tag{22}$$

with $n_{exf,m}$ the extra-fibrillar water mass fraction, and ρ_s the mass density of the solid matrix. According to Maroudas and Bannon (1981), Maroudas et al. (1991) and Urban and McMullin (1988) $n_{exf,m}$ is given by

$$n_{exf,m} = n_{f,m} - n_{inf,m} = n_{f,m} - \varphi_{ci} \rho_{c,tot,m}, \tag{23}$$

where $n_{f,m}$ and $n_{inf,m}$ are the mass fraction of total and intra-fibrillar water, respectivily, φ_{ci} a parameter that defined the

mass intra-fibrillar water per collagen mass, and $\rho_{c,tot,m}$ is the collagen mass fraction with respect to the total wet weight, which is given by

$$\rho_{c,tot,m} = (1 - n_{f,m}) \sum_{i=1}^{totf} \rho_c^i. \quad (24)$$

Maroudas et al. (1991) determined the dependence of φ_{ci} on the osmotic pressure gradient $\Delta\pi$. We fitted their data with an exponential function as

$$\varphi_{ci} = 0.448e^{-0.328\Delta\pi} + 0.822. \quad (25)$$

The osmotic pressure gradient $\Delta\pi$ from Eq. (19) is then given by

$$\Delta\pi = \phi_{int} RT \sqrt{c_{F,exf}^2 + 4\frac{\gamma_{ext}^{\pm 2}}{\gamma_{int}^{\pm 2}} c_{ext}^2} - 2\phi_{ext} RT c_{ext}, \quad (26)$$

The model was implemented in ABAQUS v6.3 (Hibbitt, Karlsson & Sorensen, Inc., Pawtucket, RI, USA). For more details about this model see Wilson et al. (2004, 2005a,b).

2.2 Composition and structure

2.2.1 Fluid fraction

Based on literature (Lipshitz et al. 1975; Shapiro et al. 2001; Rieppo et al. 2004) the fluid volume fraction was assumed to be

$$n_f = 0.9 - 0.2z^*, \quad (27)$$

where z^* is the normalized depth of the tissue (z^* is 0 at the articular surface and 1 at the bottom of the cartilage). The fluid mass fraction per total solid is than given by (Fig. 2)

$$n_{f,m} = \frac{n_f}{n_f + (1 - n_f)\rho_s}. \quad (28)$$

The mass density of the solid matrix ρ_s was assumed to be 1.43 (Basser et al. 1998; Shapiro et al. 2001).

2.2.2 Fixed charge density

The FCD was assumed to be (Maroudas 1968; Maroudas and Bannon 1981; Chen et al. 2001) (Fig. 3)

$$c_F = -0.10(z^*)^2 + 0.24z^* + 0.035. \quad (29)$$

2.2.3 Collagen content

When assuming that the total mass solid density and the collagen mass density are equal (Basser et al. 1998; Shapiro et al. 2001), the collagen mass fraction and volume fraction are the same. This collagen fraction with respect to the total solid volume was assumed to be (Rieppo et al. 2004) (Fig. 4)

$$n_{coll} = 1.4(z^*)^2 - 1.1z^* + 0.59. \quad (30)$$

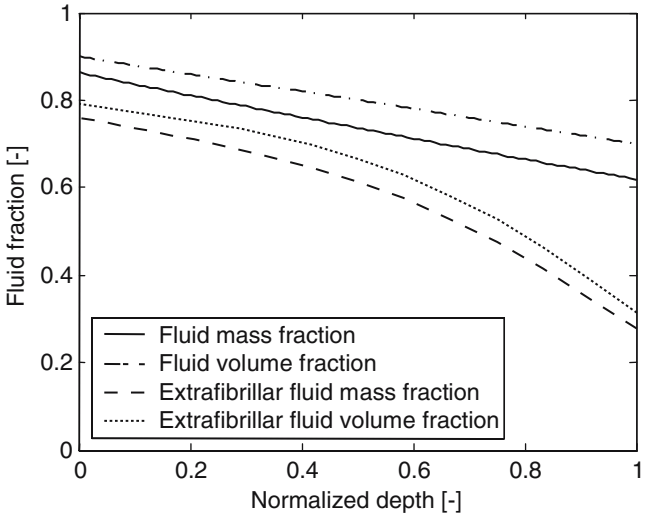

Fig. 2 Depth-dependent fluid fractions

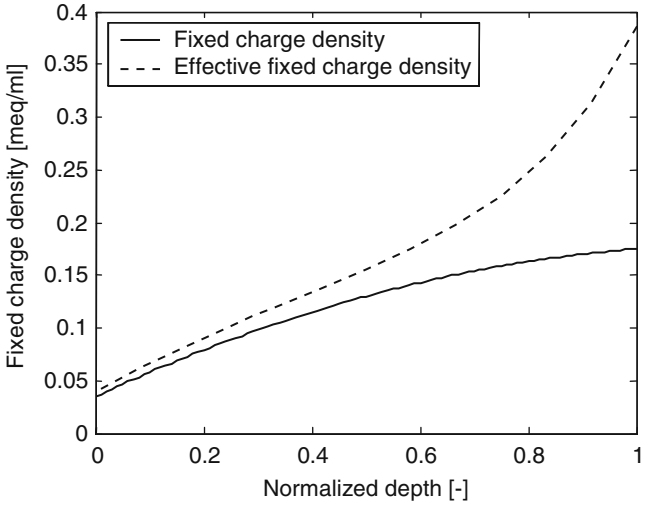

Fig. 3 Depth-dependent fixed charge densities

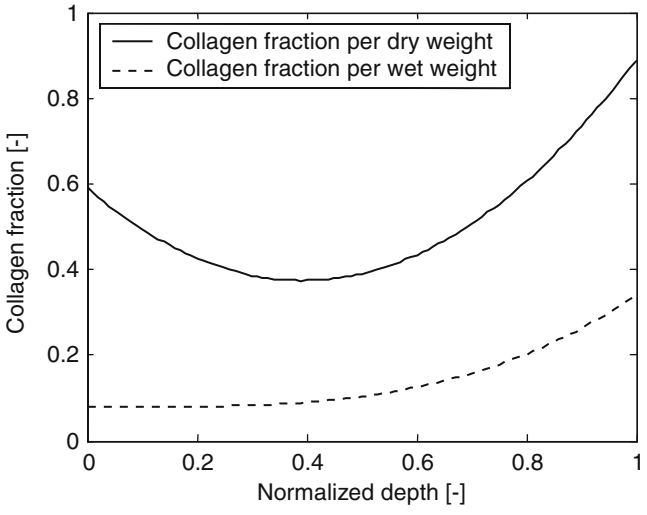

Fig. 4 Depth-dependent collagen fractions

2.2.4 Collagen structure

The 3D-collagen network was captured as a combination of large primary collagen fibrils and smaller secondary fibrils (Wilson et al. 2005b). As described in the arcade model of Benninghoff (1925), bundles of primary fibrils extend perpendicular from the subchondral bone, split up close to the articular surface into fibrils, which curve to a horizontal course, and flush with the articular surface. It was assumed that the orientation of the secondary fibrils is random. At each point it was assumed that there are two primary and seven secondary fibril directions. For more information about the implemented fibril structure the reader is referred to Wilson et al. (2005b).

It was assumed that the density of the primary fibrils was higher than that of the secondary fibrils. The fibril densities were assumed to be

$$\begin{aligned} \rho_c &= \rho_{c,tot}\tfrac{C}{2C+7} \quad \text{for the primary fibrils,} \\ \rho_c &= \rho_{c,tot}\tfrac{1}{2C+7} \quad \text{for the secondary fibrils,} \end{aligned} \tag{31}$$

with C a positive constant larger than 1, and $\rho_{c,tot}$ the depth-dependent total collagen volume fraction per total solid volume.

In the literature material properties, like fluid fraction, fixed charge density, fibril orientation and cartilage thickness are derived from measurements of cartilage in swollen equilibrium with a physical salt solution of 0.15 M NaCl.

Hence, the material parameters were implemented such that the all correspond with the situation at which the tissue is in equilibrium with a salt concentration of 0.15 M NaCl (Wilson et al. 2005b).

2.3 Determination of unknown material properties

The unknown material properties are G_m, E_1, E_2, C and k. As we are only interested in the equilibrium properties the value of the permeability k is not important, and was set a constant value of 1×10^{-15} m^4/Ns. C was taken from Wilson et al. 2005b, and set at 3.009. The remaining parameters (G_m, E_1 and E_2) were determined by fitting them to experimental data of 1D confined swelling and 1D free swelling tests The fitting procedures were performed iteratively, using a multidimensional unconstrained nonlinear minimization procedure available in Matlab Version 5.3 (The MathWorks Inc., 1984–1999). From within this Matlab procedure ABAQUS was called to simulate the experiments. The output from ABAQUS was then transferred to Matlab, after which the objective function was determined as:

$$f = \frac{1}{n}\sum_{i=1}^{n}\left(\frac{F^i_{EXP} - F^i_{FEM}}{F^i_{EXP}}\right)^2 + \frac{1}{m}\sum_{i=1}^{m}\left(\frac{\varepsilon^i_{EXP} - \varepsilon^i_{FEM}}{\max(\varepsilon_{EXP})}\right)^2, \tag{32}$$

where F_α are the reaction forces during the 1D confined swelling test, and ε_α the free swelling strains of the 1D free swelling test. The subscripts EXP and FEM refer to the experiments and model results, respectively.

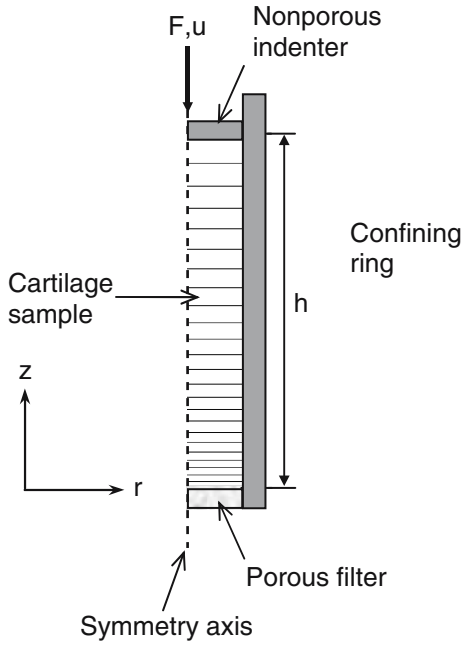

Fig. 5 1D swelling mesh ($h = 0.6$ mm) (h is the height of the cartilage sample, F the external force and u the displacement of the indenter)

2.3.1 1D confined swelling test

Eisenberg and Grodzinsky (1987) performed a 1D-swelling experiment in which they measured the swelling pressures in an axially compressed cartilage plug for different external salt concentrations. This swelling test was limited to a 1-dimensional model, using an axisymmetric finite element mesh, consisting of a single column of 25 axisymmetric pore pressure elements (CAX4P) (Fig. 5).

Since Eisenberg and Grodzinsky (1987) removed the top 2.5% and bottom 37.5% of their full thickness cartilage samples, the normalized depth z^* was set from 0.025 to 0.625. The nodal displacements at the bottom plane were confined in z-direction. The displacements of all nodes were confined in radial direction. At the top of the model, zero pore pressure was prescribed, i.e. fluid can flow in and out freely. All other surfaces were assumed to be impermeable. The mesh was axially compressed by 15%. After full relaxation, the external salt concentration was decreased to 0.0001 M. After equilibrium was reached the salt concentration was increased with steps of 0.05 M until an external salt concentration of 2 M was reached. During this process the height of the sample was held constant, while the axial reaction forces were computed.

2.3.2 1D free swelling test

In the second swelling test we measured the free swelling strains of articular cartilage as a function of the external salt

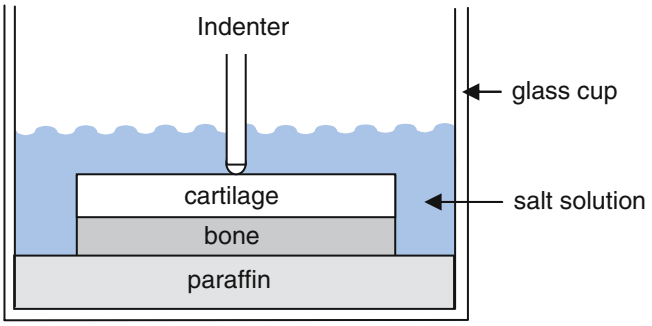

Fig. 6 Schematic of the free swelling setup. The cartilage sample was fixed in paraffin and indented with the ARES rheometer

concentration. 8 cartilage-bone samples of approximately 30 × 15 × 15 mm were sawed from fresh calf tibial plateaus. The osseous parts of the samples were fixed in paraffin in a glass cup, and the whole sample was bathed in demineralized water for three hours. Each sample was placed in a rheometer (Rheometric scientific Advanced Rheometric expansion system ARES-LS). Sample height was determined by measuring the vertical position of a spherical indenter (radius 2 mm, located above the center the sample) when it indents the sample with a contact-force of 10 μN (Fig. 6). The position of the indenter (height of the sample) was retrieved as soon as contact was established after which the indenter was immediately removed from the sample. The indentation was performed near the center of the sample, far away from its edges where the collagen network might be damaged due to sawing. The salt concentration in the cup was increased in a step-wise manner. After each increase the sample was left to equilibrate, after which the sample height was measured again. The concentrations, at which the sample height was measured, were 0.00, 0.07, 0.15, 0.30, 0.67, 1 and 2 M NaCl. The salt concentration was increased by adding a solution of 4 M NaCl.

After each test, when the samples are in equilibrium with 2 M NaCl, they were removed from the cup and the thickness of the cartilage was optically determined using a Zeiss Stemi 2000-c binocular. The thickness was measured at the same location as the indentation took place. The free swelling strains were calculated by

$$\varepsilon(\alpha) = \frac{h(\alpha) - h(2\,\mathrm{M})}{h(2\,\mathrm{M})}, \tag{33}$$

where $h(2\,\mathrm{M})$ is the cartilage thickness at 2 M, and $h(\alpha)$ is the cartilage thickness at a salt concentration α.

Because the cartilage height was on the average ten times smaller than its width, fluid flow and deformation in the center of the tissue were assumed only to occur in axial direction. The test was modeled with the same mesh as given in Fig. 6. As full thickness cartilage samples were used, the normalized depth z^* ranged from 0.0 to 1.0. The nodal displacements at the bottom plane were confined in z-direction. The displacements of all nodes were confined in radial direction. At the top of the model, zero pore pressure was prescribed, i.e. fluid can flow in and out freely. All other surfaces were assumed to be impermeable. After equilibration to 0.15 M, the external salt concentration was decreased to zero. After equilibration the salt concentration was increased to 2 M in a stepwise manner. After each step the model was left to equilibrate. After equilibration the height of the sample was recorded and the free swelling strain was computed using Eq. (33).

2.4 Determination of depth-dependent compressive equilibrium properties

The simulated depth-dependent compressive equilibrium properties were determined in the same way as has experimentally been done by Schinagl et al. (1997). They compressed osteochondral samples and allowed them to equilibrate, and measured intratissue displacement within the cartilage with fluorescently labeled chondrocyte nuclei as intrinsic, fiducial markers. Axial strain was then calculated in nine sequential 125 μm thick cartilage and in a 225 μm thick layer of cartilage adjacent to the cartilage-bone interface.

The simulation was limited to a 1-dimensional model, using an axisymmetric finite element mesh, consisting of a single column of 33 pore pressure elements (CAX4P) (Fig. 7). The total height of the mesh was 1.38 mm. The element distribution was chosen so that the model could be divided in nine layers of 0.125 mm and one layer of 0.225 mm. The displacements of all nodes were confined in radial direction. At the top of the model, zero pore pressure was prescribed, i.e. fluid can flow in and out freely. All other surfaces were assumed to be impermeable. After equilibration to 0.15 M, the

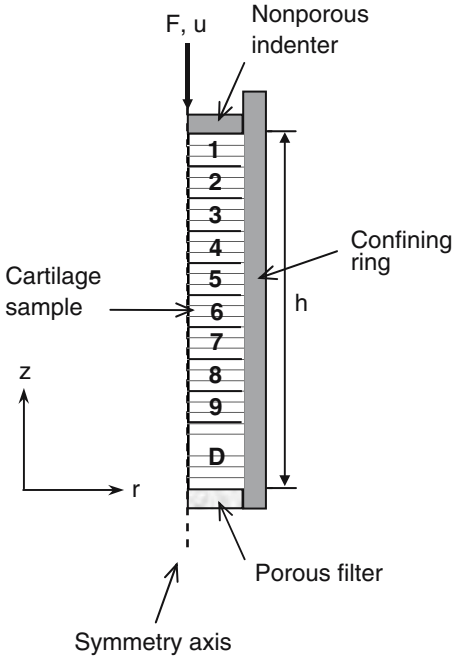

Fig. 7 Confined compression mesh ($h = 1.38$ mm). The mesh was divided into nine layers (1–9) of 0.125 mm and one deep layer (D) of 0.225 mm (h is the height of the cartilage sample, F the external force and u the displacement of the indenter)

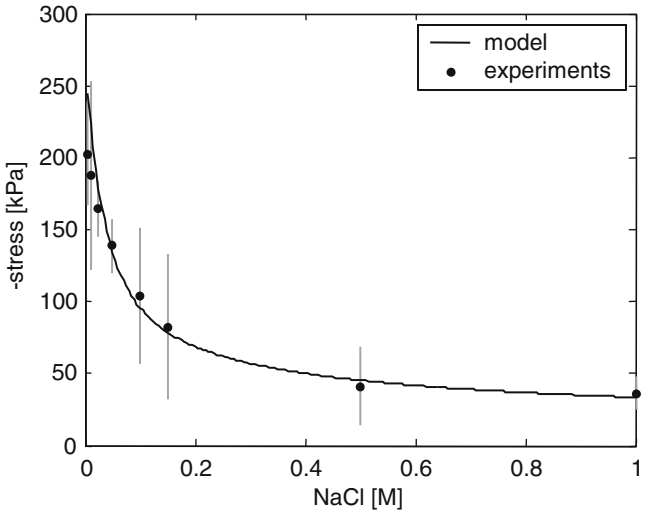

Fig. 8 Axial external pressure measured from 1D confined swelling tests (Eisenberg and Grodzinksy 1987) along with FEA-model curvefit

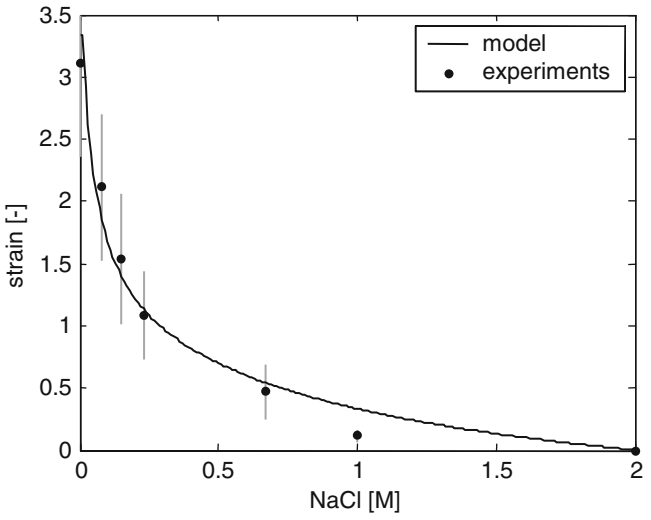

Fig. 9 Axial strain measured from 1D free swelling tests along with FEA-model curvefit

model was axially compressed in a stepwise manner. After each step the model was left to equilibrate. After equilibration the applied pressure and the strains in the nine layers was recorded.

3 Results

3.1 Determination of unknown material properties

To determine the unknown material parameters (G_m, E_1 and E_2), equilibrium reaction forces during confined 1D swelling and equilibrium free swelling strains during free swelling as computed with the model were fitted to the experimental data. The resulting model parameters characterizing normal bovine articular cartilage were determined at $G_m = 0.723\,\text{MPa}$, $E_1 = 4.63\,\text{MPa}$ and $E_2 = 3,670\,\text{MPa}$.

The model response during 1D confined and free swelling corresponds well with the experimental data (Figs. 8, 9). For both tests the coefficient of determination (R^2) was 0.98.

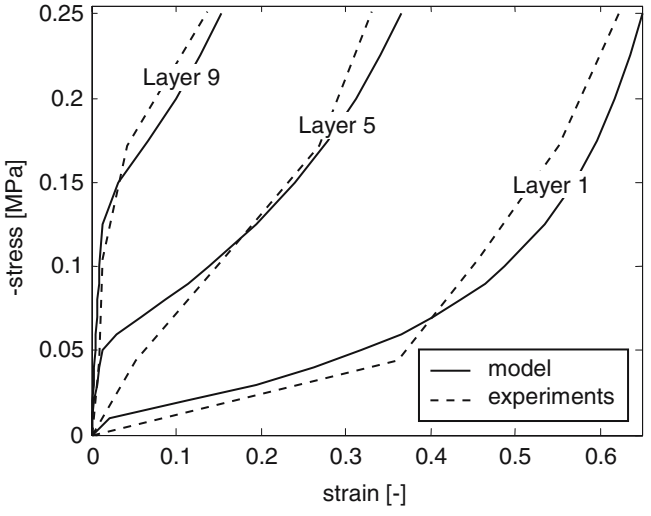

Fig. 10 Depth-dependent stress–strain behavior of articular cartilage measuring during confined compression (Schinagl et al. 1997) along with FEA-model results

3.2 Determination of depth-dependent compressive equilibrium properties

The finite element results for layer 1 and 9 correspond well with the experimental results of Schinagl et al. (1997) (Fig. 10). However, for layer 5, the stresses are overestimated for low strains (Fig. 10). From the stress–strain curves the effective aggregate modulus of the tissue was determined ($H_A = \partial\sigma/\partial\varepsilon$) (Fig. 11). For all layers the effective aggregate modulus decreases with increasing strain for low strains then reaches a deflection point after which the effective aggregate modulus start to increase with increasing strain. For all layers this deflection point lies around 4% strain.

To be able to explain the strain-dependent behavior over the height of the tissue, the osmotic pressure gradient, the stress in z-direction in the non-fibrillar matrix, the fibrillar matrix and the total tissue were plotted as a function of tissue strain for layer 1 and 9 (Fig. 12). In layer 9 the osmotic pressure is very high (around 0.15 MPa). The high osmotic pressure in layer 9 is counter balanced by the fibril stresses and external load. Initially this is collagen fibrils carry most of the load but as the external load increases, the amount load carried by the fibrils decreases. At an external load of 0.15 MPa the fibrillar stress is reduced to zero. The non-fibrillar matrix stress is unaffected by these changes and shows the same behavior as seen in Fig. 1. For layer 1 the same trends can be seen, although they are less pronounced.

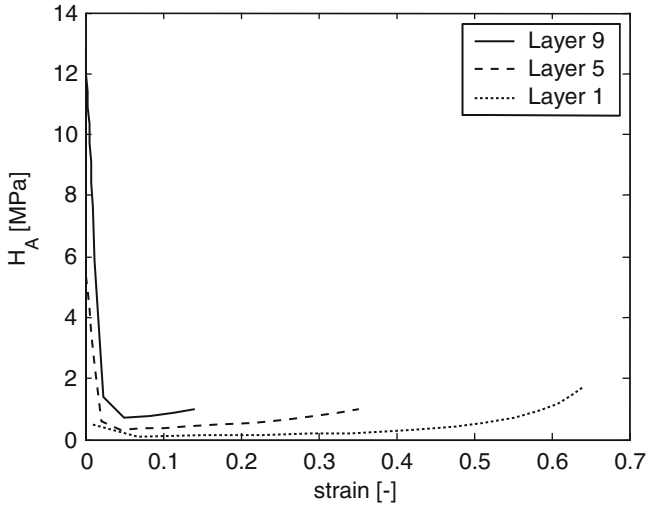

Fig. 11 Strain-dependent effective aggregate modulus (H_A) for different layers of articular cartilage as computed with the FEA-model

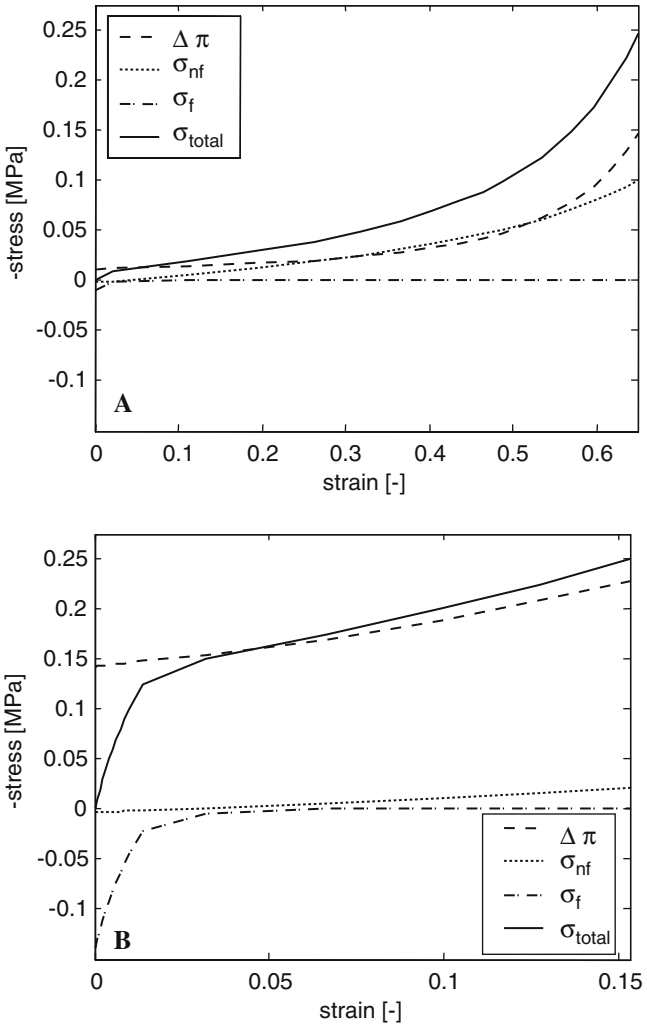

Fig. 12 Stress–strain behavior of the different components of articular cartilage, for layer 1 (**a**) and layer 9 (**b**) as computed with the FEA-model

4 Discussion

For this study we hypothesized that the depth-dependent compressive equilibrium properties of articular cartilage are the inherent consequence of the composition of the tissue, which changes with depth. To test this hypothesis our recently developed fibril-reinforced poroviscoelastic swelling model (Wilson et al. 2005b) was expanded to include the influence of intra- and extra-fibrillar water content, and the influence of the solid fraction on the compressive properties of the tissue. In the model the composition and collagen orientation were depth-dependent, while the material constants for the individual components were constant over the height of the tissue. It was shown that with this model the typical depth-dependent behavior of articular cartilage can be described.

One of the most important changes to the model of Wilson et al. (2005b) was the inclusion of the influence of intra- and extra-fibrillar water. The difference between the total fluid content and extra-fibrillar content (100% × (extra-fibrillar water–total water)/(total water)), increased from –12% at the articular surface to–55% in the deep zone. This depth-dependent difference in fluid content had a great effect on the depth-dependency of the effective FCD. The difference between the measured and effective FCD increased from 13% at the articular surface to 122% in the deep zone. Maroudas and Bannon (1981) found similar differences experimentally. However, our deep zone effect exceeds their values. This is due the high collagen content in the deep zone used in the model. The collagen content used in this study was from Rieppo et al. (2004). They measured the collagen content in young bovine patellae, while Maroudas and Bannon (1981) and Maroudas et al. (1991) measured the collagen content in human tibial or femoral head cartilage. As the experiments of Schinagl et al. (1997) were performed on young bovine femoral-groove cartilage, using the data from Rieppo et al. (2004) is more appropriate in this study. As the swelling pressures are directly related to the effective FCD, it can be concluded that the effect of intra- and extra-fibrillar fluid on the swelling pressures in articular cartilage is very high. It was shown that the resulting depth-dependent swelling pressures can for a large part account for the strain-dependent effective equilibrium stiffness of articular cartilage.

The effective aggregate modulus showed a highly strain-dependent behavior. The effective aggregate modulus decreases with increasing strain for low strains, reaching a deflection point after which the effective aggregate modulus starts to increase with increasing strain. This effect becomes more pronounced with increasing distance from the articular surface. The deflection point marks the point at which the external load exceeds the local osmotic pressure gradient. Due to the high FCD in the deep zone, the deflection point in the effective stiffness occurs at higher external pressures in the deep zone than at the surface. Due to the initial swelling pressures the cartilage is initially under tension.

Only when the deflection point is reached the tissue becomes compressed. Hence, the stress–strain relation at strains below the deflection point represents the tensile stiffness of the tissue, and the stress–strain relation after the deflection point represents the compressive stiffness. This confirms the hypothesis of Chahine et al. (2004) that the stain-softening in articular cartilage is the consequence of compression–tension nonlinearity in the presence of osmotic swelling.

In the unloaded state, the swelling pressures are counter balanced by the collagen fibrils. Hence, the swelling pressure inside articular cartilage is high. Is was shown that due to the intra-fibrillar fluid, which is trapped between the collagen fibrils, the effective FCD and thereby the swelling pressures are increased (Urban and McMullin 1988; Maroudas and Bannon 1981; Katz et al. 1986; Maroudas et al. 1991. Through this mechanism the collagen fibrils also directly contribute to the swelling pressures. The current study shows how important this mechanism is for stress distributions over the height of articular cartilage.

Other depth-dependencies that were added to the model of Wilson et al. (2005b) were the solid fraction dependency of the stiffness and compressibility of the non-fibrillar matrix. This solid fraction dependency mainly influenced the strain-dependent behavior of the tissue above the aforementioned deflection point in the stress–strain curve.

Unfortunately, limited availability of literature data forced us to base the depth-dependent composition on data for cartilage from different species which were determined in distinct studies (Maroudas 1968; Lipshitz et al. 1975; Maroudas and Bannon 1981; Chen et al. 2001; Shapiro et al. 2001; Rieppo et al. 2004). A mismatch in composition between the samples used in these studies may account for differences between the experimental and numerical results in the present study, or might have resulted in an error in the obtained material constants. Note that the depth-dependent properties as found by Schinagl et al. (1997) are the result of a completely different study than the studies from which we used data to determine the material properties for the model. Even though the data from Schinagl et al. (1997) was not used in any way as input for the current model, the correspondence between their depth-dependent data and our model properties are very accurate. This indicated the validity of the present approach.

During cartilage degeneration and tissue engineering the mechanical properties of the tissue changes as its composition changes. Since in the present model the mechanical properties of the tissue are the direct consequence of the composition of the tissue, these changes in composition can be directly accounted for.

In conclusion using a fibril-reinforced poroviscoelastic swelling model, including the influence of intra- and extrafibrillar water content and the influence of the solid fraction on the compressive properties of the tissue, it was shown that the depth-dependent compressive equilibrium properties during confined compression of articular cartilage can be explained by its composition. The main insight from this study is that the depth-dependent compressive properties during confined compression of articular cartilage can be obtained from its depth-dependent composition, only. This eliminates the need for the assumption that the material properties of the different constituents themselves vary with depth. Such insights are important for understanding cartilage mechanical behavior, cartilage damage mechanisms and tissue engineering studies.

Acknowledgements This project was supported by a grant from the AO Foundation, Switzerland.

References

Armstrong CC, Mow VC (1982) Variations in the intrinsic mechanical properties of human articular cartilage with age, degeneration, and water content. J Bone Joint Surg Am 64(1):88–94

Basser PJ, Schneiderman R, Bank RA, Wachtel E, Maroudas A (1998) Mechanical properties of the collagen network in human articular cartilage as measured by osmotic stress technique. Arch Biochem Biophys 351(2):207–219

Benninghoff A (1925) Form und Bau der Gelenkknorpel in ihren Beziehungen zur Funktion. Z Zellforsch 2:783–862

Buckwalter JA, Hunziker EB, Rosenberg LC, Coutts R, Adams M, Eyre D (1991) Articular cartilage: Composition and structure. In: Wo Sl, Buckwalter JA (eds) Injury and repair of musculoskeletal soft tissues, 2nd edn. American Acedemy of Orthopaedic Surgeons, Park Ridge 405–425

Chahine NO, Wang CC, Hung CT, Atheshian GA (2004) Anisotropic strain-dependent material properties of bovine articular cartilage in the transitional range from tension to compression. J Biomech 37(8):1251–1261

Charlebois M, McKee MD, Buschmann MD (2004) Nonlinear tensile properties of bovine articular cartilage and their variation with age and depth. J Biomech Eng 126(2):129–137

Chen SS, Falcovitz YH, Schneiderman R, Maroudas A, Sah RL (2001) Depth-dependent compressive properties of normal aged human femoral head articular cartilage: relationship to FCD. Osteoarthritis Cartilage, 9:561–569

Clark JM (1991) Variation of collagen fiber alignment in a joint surface: a scanning electron microscope study of the tibial plateau in dog, rabbit, and man. J Orthop Res 9:246–257

Clarke IC (1971) Articular cartilage: a review and scanning electron microscope study. 1. The interterritorial fibrillar architecture. J Bone Joint Surg Br 53:732–750

Ehlers W, Eipper G (1999) Finite elastic deformations in liquid-saturated and empty porous solids. Trans Porous Media 34:179–191

Eisenberg SR, Grodzinsky AJ (1987) The kinetics of chemically induced nonequilibrium swelling of articular cartilage and corneal stroma. J Biomech Eng 109:79–89

Hasler EM, Herzog W, Wu JZ, Muller W, Wyss U (1999) Articular cartilage biomechanics: theoretical models, material properties, and biosynthesis response. Clin Rev Biomech Eng 27:415–488

Hunziker E (1992) Articular artilage structure in humans and experimental animals. In: Kuettner KE, Peyron JG, Schleyer R, Hascall VC, (eds) articular cartilage and osteoarhritis. Raven Press, New York, 183–199

Hunziker EB, Michel M, Studer D (1997) Ultrastructure of adult human cartilage matrix after cryotechnical processing. Microsc Res Tech 37:271–284

Huyghe JM, Houben GB, Drost MR, van Donkelaar CC (2003) An ionised/non-ionised dual porosity model of intervertebral disc tissue. Biomech Model Mechanobiol 2:3–19

Katz EP, Wachtel EJ, Maroudas A (1986) Extra-fibrillar proteoglycans osmotically regulate the molecular packing of collagen in cartilage. Biochim Biophys Acta 882:136–139

Lanir Y (1987) Biorheology and fluid flux in swelling tissues. I. Bicomponent theory for small deformations, including concentration effects. Biorheology 24:173–187

Lipshitz H, Etheridge R, Glimcher MJ (1975) In vitro wear of articular cartilage. J Bone Joint Surg 57:527–537

Maroudas A (1968) Physicochemical properties of cartilage in the light of ion exchange theory. Biophys J 8:575–595

Maroudas A, Bannon C (1981) Measurement of swelling pressure in cartilage and comparison with the osmotic pressure of constituent proteoglycans. Biorheology 18:619–632

Maroudas A, Wachtel E, Grushko G, Katz EP, Weinberg P (1991) The effect of osmotic and mechanical pressures on water partitioning in articular cartilage. Biochim Biophys Acta 1073:285–294

Meyer FA (1983) Macromolecular basis of globular protein exclusion and of swelling pressure in loose connective tissue (umbilical cord). Biochim Biophys Acta 755:388–399

Mow VC, Guo XE (2002) Mechano-electrochemical properties of articular cartilage: their inhomogeneities and anisotropies. Annu Rev Biomed Eng 4:175–209

Mow VC, Kuei SC, Lai WM, Armstrong CG (1980) Biphasic creep and stress relaxation of articular cartilage in compression: theory and experiments. J Biomech Eng 102:73–84

Mow VC, Zhu W, Ratclife A (1991) Structure and function of articular cartilage and meniscus. In: Mow VC, Hayes WC (eds). Basic orthopaedic biomechanics. Raven Press, New York, 143–198

Rieppo J, Hyttinen MM, Lappalainen R, Jurvelin JS, Helminen HJ (2004) Spatial determination of water, collagen and proteoglycan contents by Fourier transform infrared imaging and digital densitometry. Trans ORS, 1021

Rieppo J, Töyräs J, Nieminen MR, Jurvelin JS, Helminen HJ (2005) Spatial mapping of cartilage collagen and proteoglycans by FT-IRS. Trans ORS, 1484

Sah RL, Yang AS, Chen ACm Haut JJ, Halili RB, Yoshioka M, Amiel D, Coutts RD (1997) Physical properties of rabbit articular cartilage after transection of the anterior cruciate ligament. J Orthop Res 15(2):197–203

Schinagl RM, Gurskis D, Chen AC, Sah RL (1997) Depth-dependent confined compression modulus of full-thickness bovine articular cartilage. J Orthop Res 15:499–506

Shapiro EM, Borthakur A, Kaufman JH, Leigh JS, Reddy R (2001) Water distribution patterns inside bovine articular cartilage as visualized by 1H magnetic resonance imaging. Osteoarthritis Cartilage 6:533–538

Truesdell C, Toupin R (1960) The classical field theories, Handbuck der Physik II/I. Springer, Berlin Heidelberg New York

Urban JPG, Maroudas A, Bayliss MT, Dillon J (1979) Swelling pressures of proteoglycans at the concentrations found in cartilagenous tissues. Biorheology 16:447–464

Urban JPG, McMullin JF (1988) Swelling pressures of the lumbar intervertebral discs: influence of age, spinal level, composition and degeneration. Spine 13:179–187

Wilson W, van Donkelaar CC, Huyghe JM (2005a) A Comparison between mechano-electrochemical and biphasic swelling theories for soft hydrated tissues. J Biomech Eng 127:158–165

Wilson W, van Donkelaar CC, van Rietbergen B, Huiskes R (2005b) A fibril-reinforced poroviscoelastic swelling (FPVES) model for articular cartilage. J Biomech 38:1195–1204

Wilson W, van Donkelaar CC, van Rietbergen C, Ito K, Huiskes R (2004) Stresses in the local collagen network of articular cartilage: a poroviscoelastic fibril-reinforced finite element study. J Biomech 37:357–366

Wong M, Wuethrich P, Eggli P, Hunziker EB (1996) Zone-specific cell biosynthesis activity in mature bovine articular cartilage: a new method using confocal microscopic stereology and quantitative autoradiography. J Orthop Res 14:424–432